ChemComm

COMMUNICATION

View Article Online
View Journal | View Issue

Cite this: *Chem. Commun.*, 2021, 57, 9926

Received 19th July 2021,
Accepted 23rd August 2021

DOI: 10.1039/d1cc03870b

rsc.li/chemcomm

Chiral porous CN-bridged coordination polymer mimicking MOF-74 and showing magnetization photoswitching†

Michał Magott * and Dawid Pinkowicz *

A chiral porous cyanide-bridged framework $\{[Mn^{II}(L)]_2[W^{IV}(CN)_8]\cdot 10H_2O\}_n$ (1; L = 2,6-bis[1-(2-(*N*-methylamino)ethylimino)ethyl]-pyridine) showing a strong structural similarity to MOF-74 has been prepared and characterised. The crystallised water molecules can be easily removed below 60 °C, leading to a distinct crystal colour change and the activation of its photomagnetic properties – constituting the so called photomagnetic sponge behaviour of this system. The complete dehydration of 1 proceeds through a single-crystal-to-single-crystal transformation and the resulting anhydrous framework $\{[Mn^{II}(L)]_2[W^{IV}(CN)_8]\}_n$ (1anh) was studied using single-crystal X-ray diffraction.

Metal–organic frameworks (MOFs), coordination polymers characterised by metal nodes connected by organic linkers, are regarded as the new generation of "smart" sorption materials. Terephthalate-based MOFs seem to attract most of the attention,[1] with MOF-74 being the prominent example of a material characterised by a remarkable stability of the coordination network and unique sorption properties.[2] The modular characteristics of its skeleton, constructed from divalent metal cations and 2,5-dihydroxybenzene-1,4-dicarboxylate, were utilized to tailor specific functionalities, such as the sorption of carbon dioxide,[3–5] conductivity[6–8] or gas separation.[9,10] One of the approaches to further improve the properties of this framework is based on its decoration with a specifically designed mixture of active metal sites.[11,12]

Herein, we demonstrate a cyanide-bridged coordination polymer $\{[Mn^{II}(L)]_2[W^{IV}(CN)_8]\cdot 10H_2O\}_n$ (**1**; L = 2,6-bis[1-(2-(*N*-methylamino)ethylimino)ethyl]-pyridine), see Fig. S1 in the ESI†) mimicking the topology of MOF-74 despite a completely different preparation strategy involving the use of an octacyanometallate anion as a linker. Octacyanometallates in combination with cationic transition metal complexes are known to form functional bimetallic three-dimensional (3-D) coordination polymers (CPs) by design.[13] Chirality of the CPs is usually achieved by the intentional incorporation of chiral ligands at the self-assembly stage[14–16] and the crystallisation of chiral CPs from achiral building blocks is unexpected and rare.[17,18] In the particular case of **1** the combination of $[W^{IV}(CN)_8]^{4-}$ with achiral $[Mn^{II}(L)]^{2+}$ serendipitously leads to a unique chiral CP that not only mimics MOF-74's topology and porosity, but also shows single-crystal-to-single-crystal (SCSC) transformation induced by water sorption, different photomagnetic behaviour depending on the hydration level and spontaneous resolution of the enantiomeric forms by crystallisation.

Compound **1** crystallises in the form of dark yellow needle crystals from a water–acetonitrile solution comprising $[Mn^{II}(L)]Cl_2$ and $K_4[W^{IV}(CN)_8]\cdot 2H_2O$ (see the Experimental section of the ESI† for details). Its 3-D coordination framework in the trigonal crystal system shows a strong resemblance to MOF-74 (Fig. 1a and b). Crystals of **1** consist of $-Mn^{II}(L)$-(μ-NC)-$W^{IV}(CN)_6$-(μ-CN)– helical rods running along the *c* direction, with the octacyanotungstate(IV) moieties connecting the neighbouring rods. Contrary to MOF-74 crystallising in a centrosymmetric $R\bar{3}$ space group, **1** undergoes a spontaneous resolution into a racemic mixture of enantiopure crystals in two enantiomorphic space groups: $P3_121$ and $P3_221$. The homochirality of the single crystals of **1** is related to the aforementioned 3_1 or 3_2 helical rods within the crystal (Fig. S2, ESI†), similar to the chiral $[Mn_3(HCOO)_4(D\text{-Cam})]_n$ MOF.[19] We hypothesize that chirality is transferred from one helix to another by flexible $[W(CN)_8]$ linkers, which are directly incorporated into both helical rods, in contrast to the rigid organic linkers simply connecting the well-separated inorganic SBUs of opposite handedness in the structure of MOF-74.[20] The chirality of a single cyanide-bridged helix may originate from the conformation of the N-CH_3 groups of the ligand, similar to the $[Mn^{II}(L)(H_2O)]_2[Mo^{III}(CN)_7]\cdot 6H_2O$ molecules, which crystallise in the chiral $P2_1$ space group.[21] Moreover, the ligand itself attains a slightly helical conformation of donor atoms, which

Faculty of Chemistry, Jagiellonian University, Gronostajowa 2, 30-387 Kraków, Poland. E-mail: michal.magott@uj.edu.pl, dawid.pinkowicz@uj.edu.pl

† Electronic supplementary information (ESI) available: Experimental details, thermogravimetric analysis, powder X-ray diffraction patterns, magnetic measurements, UV-vis, and IR spectra and CIF files. CCDC 2094734 (**1** right-handed), 2094735 (**1** left-handed), 2094736 (**1anh** right-handed). For ESI and crystallographic data in CIF or other electronic format see DOI: 10.1039/d1cc03870b

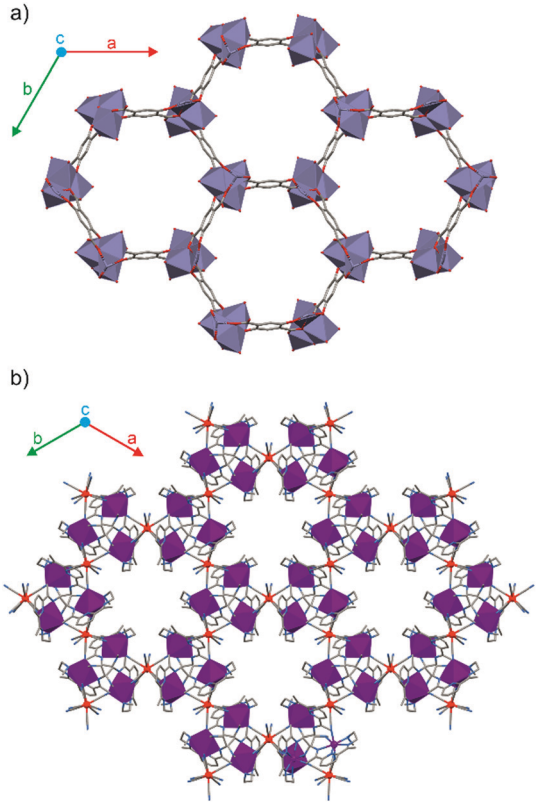

Fig. 1 Fragments of the crystal structure demonstrating the coordination framework of MOF-74 (a) and **1** ($P3_121$ enantiomer) (b) as seen along the crystallographic *c* axis.

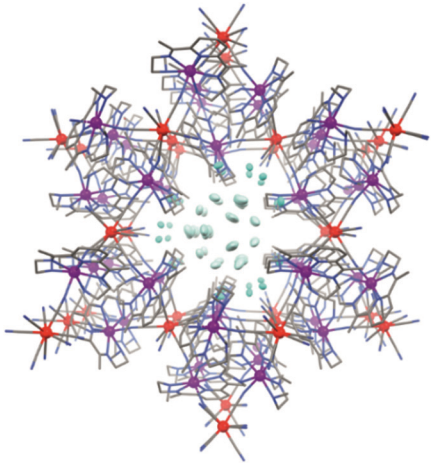

Fig. 2 Fragments of the crystal structure demonstrating water molecules forming hydrogen bonds with cyanides (cyan) as well as water molecules occupying the interior of the pores (light blue) in **1**. W – red, Mn – purple, N – dark blue, C – grey.

may be associated with the twist of the helices forming the coordination skeleton (Fig. S2, ESI†). In the crystal structure of **1** there are two types of water molecules: four molecules per Mn_2W formula unit form direct hydrogen bonds with the nitrogen atoms of the terminal cyanide ligands and the remaining six molecules occupy the interior of the pores (Fig. 2). The crystallised water molecules in the structure of **1** can be completely removed below 60 °C, as demonstrated by the thermogravimetric analysis (TGA) under a dry nitrogen atmosphere (Fig. S3, ESI†). The anhydrous coordination framework is stable up to 250 °C, which is uncommon for this class of compounds.[22] A clear step-like feature at 270 °C marks the decomposition temperature of anhydrous $\{[Mn^{II}(L)]_2[W^{IV}(CN)_8]\}_n$ (**1anh**). Interestingly, the dehydrated crystals of **1** do not show any signs of deterioration (no cracking or turning opaque) and preserve their chirality. Nevertheless, the single-crystal X-ray diffraction pattern for anhydrous $\{[Mn^{II}(L)]_2[W^{IV}(CN)_8]\}_n$ (**1anh**) is characterised by a relatively high mosaicity, hence, it is difficult to obtain a good-quality structural model for large crystals of **1anh** using a commercial diffractometer. The determination of the crystal structure was possible for a very small crystal of **1anh** using synchrotron radiation at 30 K (Diamond Light Source, United Kingdom). Comparison of the structural models of **1** and **1anh** (Tables S1, S2 and Fig. S4, S5, ESI†) indicates that the dehydration process only slightly affects the cyanide-bridged framework and the conformation of the organic ligands. The unit cell volume at room temperature shrinks from 4005.8(2) Å^3 for **1** to 3786.3(7) Å^3 for **1anh** upon dehydration (data based on the Pawley analysis of the experimental PXRD patterns; for details see Fig. S6 and S7 in the ESI†). Interestingly, the *a* period related to the opening of the channels shrinks by 2.1% as compared to the 1.4% decrease of the *c* period upon dehydration. This results in the stability of the material, which loses and reabsorbs water reversibly in at least three dehydration–rehydration cycles as demonstrated by the powder X-ray diffraction studies (PXRD) (Fig. S8, ESI†). The most pronounced difference between the PXRD for **1** and **1anh** is an approximately 50% line broadening for the latter (Fig. S9, ESI†), which most probably results from the crystal lattice distortion induced by water removal. This is supported by the narrowing of the diffraction peaks upon rehydration, which also confirms that there is no permanent damage associated with the H_2O removal.

The desorption/adsorption of water was also studied using IR spectroscopy. Fig. S10 (ESI†) shows the spectra recorded in three consecutive dehydration/rehydration cycles. Each dehydration leaves the skeletal vibrations in the fingerprint region unaffected and very similar to the precursor $[Mn^{II}(L)]Cl_2{\cdot}H_2O$ (Fig. S11, ESI†), but leads to the disappearance of the broad O–H bands in the 3600–3000 cm^{-1} region – in line with the complete desorption of H_2O. Dehydration also causes a slight shift of the cyanide stretching vibration bands from 2106 cm^{-1} for **1** to 2097 cm^{-1} for **1anh**. Each rehydration results in the complete recovery of the initial IR spectrum: the O–H bands reappear and the C$\equiv$N bands shift back to 2106 cm^{-1}. This confirms the reversibility of the water sorption properties in **1**.

The porosity of powdered **1anh** was experimentally confirmed by the type I nitrogen adsorption isotherm at 77 K (Fig. S12, ESI†). Its total surface area S_{BET} = 270.1(5) m^2 g^{-1} is very similar to the 264 m^2 g^{-1} reported for the chiral Zn-MOF-74-L-Pro, but significantly smaller than the 1168 m^2 g^{-1} observed for the archetypical Zn-MOF-74.[20] The *t*-plot analysis of N_2 sorption yields a micropore volume V_{micro} = 0.0749(8) cm^3 g^{-1},

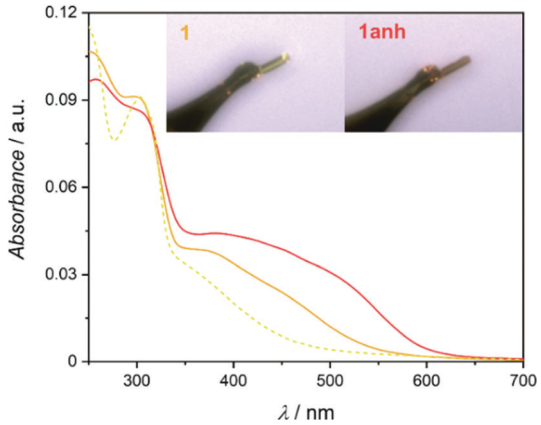

Fig. 3 Solid state UV-vis spectra for **1** (solid orange line), **1anh** (solid red line) and $Mn^{II}(L)Cl_2{\cdot}H_2O$ (dashed yellow line) at room temperature. Insets show photographs of **1** and **1anh** recorded at 100 K.

which corresponds to 10.6% of the unit cell volume. This value is smaller than the 17% volume of voids determined for **1anh** using Mercury 2020.3.0 (contact surface; probe radius 1.8 Å, grid spacing 0.5 Å).[23] However, the contact surface by definition accounts for the volume in the crystal that is accessible to the single probe molecule moving inside the pore, whereas in the nitrogen adsorption measurement some space may be blocked by already adsorbed molecules. This would explain the smaller experimental microporosity than that derived from the crystal structure.

Despite the fact that the removal of H_2O from **1** only weakly influences the entire framework, it leads to pronounced changes in its physical properties. The crystals change colour from yellow to orange-red upon dehydration (Fig. 3 inset), which is reflected in the change of the UV-vis spectra (red solid line for **1anh** *vs.* orange solid line for **1** in Fig. 3). Such changes cannot be attributed to the octacyanotungstate(IV) moiety, which does not show intense absorption bands above 500 nm (Fig. S13, ESI†).[24] On the other hand, the absorption band observed for **1anh** stretches up to 600 nm, which is much further than in the case of the $Mn^{II}(L)Cl_2{\cdot}H_2O$ precursor (yellow dashed line in Fig. 3). Such a decrease in the energy of the d–d transition is unexpected upon substitution of chloride with a strong field ligand – cyanide, especially as there are no systematic changes in the Mn^{II}–N bond lengths between the precursor $[Mn^{II}(L)Cl_2]{\cdot}1.78EtOH{\cdot}0.22H_2O$,[25] the pristine **1** and **1anh** (Table S2, ESI†). Therefore we attribute this broad and relatively intense absorption to the metal-to-ligand charge transfer band (MLCT). The energy of the CT transition often depends on the solvent,[26,27] which explains the colour change upon dehydration, despite negligible changes in the coordination environment of Mn^{II}.

The presence of the Mn^{II} nodes (S = 5/2) makes **1** and **1anh** paramagnetic. These paramagnetic centres are relatively well separated, and both phases show no signs of long range magnetic ordering down to 2 K (detailed description of their ground state magnetic properties can be found in Fig. S14 and S15 in the ESI†). However, octacyanometallates based on molybdenum(IV) or tungsten(IV) have been demonstrated to show photomagnetic effects associated with the transition from the diamagnetic S = 0 to the paramagnetic S = 1 state upon blue light irradiation.[28–31] In our previous work we have demonstrated that in $\{[Mn^{II}(imH)]_2[W^{IV}(CN)_8]\}_n$ this can lead to photo-induced magnetic ordering with the critical temperature as high as 93 K and the emergence of the magnetic hysteresis above the boiling point of liquid nitrogen.[32] We have also demonstrated that this photomagnetic effect is completely quenched after water adsorption, constituting the first "photomagnetic sponge" example. Taking into account the reversible water sorption in **1**, we decided to investigate its photomagnetic behaviour. Similar to the previously reported hydrated $\{[Mn^{II}(imH)(H_2O)_2]_2[W^{IV}(CN)_8]{\cdot}4H_2O\}_n$, **1** is completely unaffected by the 450 nm light irradiation at 10 K (P = 6–10 mW cm^{-2}; 15 h), as demonstrated in Fig. S16 (ESI†). Hence the field-cooled magnetization curve recorded after illumination closely resembles the measurement for the non-irradiated sample (Fig. S17, ESI†). On the other hand, **1anh** shows an almost five-fold increase of the magnetization after 48 hours of 450 nm irradiation at 10 K (Fig. S16, ESI†). Moreover, the photo-induced state shows bifurcation of the field-cooled and zero field-cooled magnetization curves at T_c = 48 K (Fig. 4). This remarkably high photo-induced magnetic ordering temperature is bested only by the aforementioned $\{[Mn^{II}(imH)]_2[M^{IV}(CN)_8]\}_n$ family of photomagnets (M = Mo with T_c = 72 K and M = W with T_c = 93 K, respectively)[32,33] and matches that of the $\{[Co^{II}(4\text{-Mepy})(pym)]_2[Co^{II}(H_2O)_2][W^{V}(CN)_8]_2{\cdot}4H_2O\}_n$ system[34] which is characterised by the same magnetic ordering temperature of 48 K. Due to the long-range magnetic ordering, **1anh** in its photo-induced state shows distinct magnetic hysteresis at 2 K (Fig. S18 and S19, ESI†), characterised by the coercive field of H_c = 550 Oe, remanence M_r = 0.6 Nβ and saturation magnetisation M_s = 8.8 Nβ. In the case of **1anh** the transition to the photo-induced state is not completely reversible – after 2 hours at 300 K a clear χT maximum of 15.6 cm^3 K mol^{-1} is still observed at 6.8 K (Fig. S20, ESI†) suggesting that the relaxation of the photo-induced high-spin W(IV) is not complete at room temperature. In an attempt to characterise the structure of the photo-induced state and understand the photoswitching

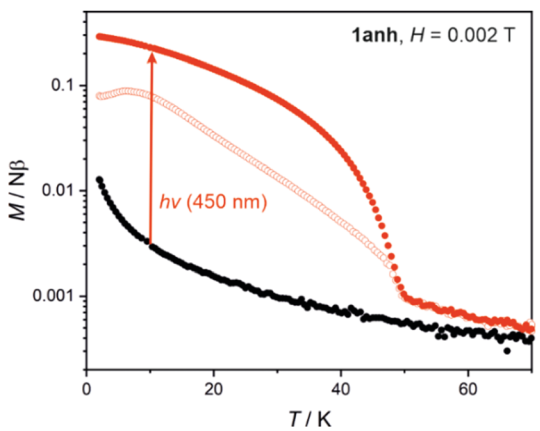

Fig. 4 Field-cooled (full circles) and zero field-cooled (open circles) magnetization curves for **1anh** before irradiation (black) and after a 450 nm light irradiation (red).

mechanism, we have performed photo-crystallography experiments on **1anh** using synchrotron radiation (Diamond Light Source, beamline I19) and prepared the elusive heptacyanotungstate(IV) complex anion[35] by photo-irradiation of octacyanotungstate(IV) (new photochemical route). Details of these experiments and the crystal structure of the photoproduct can be found in the Photomagnetic irreversibility section of the ESI.†

In summary, we have demonstrated a multifunctional CN-bridged CP that topologically mimics MOF-74. Its multifunctionality is associated with three key features: porosity, chirality and photomagnetism, which are expected to be strongly intertwined *e.g.* the guest-induced single-crystal-to-single-crystal transformation results in the ''photomagnetic sponge behaviour'' accompanied by a colour change. Further studies of the sorption properties, including possible chiral separation[36,37] and magneto-chiral effects are underway.[38,39]

This work was financed by the Polish Ministry of Science and Higher Education within the Diamond Grant project (0192/DIA/2017/46) and the National Science Centre Poland within the Opus project 2020/37/B/ST5/02735. The authors acknowledge the Diamond Light Source beamtime (proposal no. CY24501-1) and the assistance of the I19 staff.

Conflicts of interest

There are no conflicts to declare.

Notes and references

1 J. Winarta, B. Shan, S. M. McIntyre, L. Ye, C. Wang, J. Liu and B. Mu, *Cryst. Growth Des.*, 2020, **20**, 1347–1362.
2 N. L. Rosi, J. Kim, M. Eddaoudi, B. L. Chen, M. O'Keeffe and O. M. Yaghi, *J. Am. Chem. Soc.*, 2005, **127**, 1504–1518.
3 A. R. Millward and O. M. Yaghi, *J. Am. Chem. Soc.*, 2005, **127**, 17998–17999.
4 D.-A. Yang, H.-Y. Cho, J. Kim, S.-T. Yang and W.-S. Ahn, *Energy Environ. Sci.*, 2012, **5**, 6465–6473.
5 T. M. McDonald, W. R. Lee, J. A. Mason, B. M. Wiers, C. S. Hong and J. R. Long, *J. Am. Chem. Soc.*, 2012, **134**, 7056–7065.
6 W. J. Phang, W. R. Lee, K. Yoo, D. W. Ryu, B. Kim and C. S. Hong, *Angew. Chem., Int. Ed.*, 2014, **53**, 8383–8387.
7 L. Sun, C. H. Hendon, M. A. Minier, A. Walsh and M. Dincă, *J. Am. Chem. Soc.*, 2015, **137**, 6164–6167.
8 M. K. Sarango-Ramírez, D.-W. Lim, D. I. Kolokolov, A. E. Khudozhitkov, A. G. Stepanov and H. Kitagawa, *J. Am. Chem. Soc.*, 2020, **142**, 6861–6865.
9 D. Britt, H. Furukawa, B. Wang, T. G. Glover and O. M. Yaghi, *Proc. Natl. Acad. Sci. U. S. A.*, 2009, **106**, 20637–20640.
10 E. D. Bloch, L. J. Murray, W. L. Queen, S. Chavan, S. N. Maximoff, J. P. Bigi, R. Krishna, V. K. Peterson, F. Grandjean, G. J. Long, B. Smit, S. Bordiga, C. M. Brown and J. R. Long, *J. Am. Chem. Soc.*, 2011, **133**, 14814–14822.
11 L. J. Wang, H. Deng, H. Furukawa, F. Gándara, K. E. Cordova, D. Peri and O. M. Yaghi, *Inorg. Chem.*, 2014, **53**, 5881–5883.
12 Z. Ji, T. Li and O. M. Yaghi, *Science*, 2020, **369**, 674–680.
13 S. Chorazy, J. J. Zakrzewski, M. Magott, T. Korzeniak, B. Nowicka, D. Pinkowicz, R. Podgajny and B. Sieklucka, *Chem. Soc. Rev.*, 2020, **49**, 5945–6001.
14 K. Inoue, H. Imai, P. S. Ghalsasi, K. Kikuchi, M. Ohba, H. Ōkawa and J. V. Yakhmi, *Angew. Chem., Int. Ed.*, 2001, **40**, 4242–4245.
15 J. Milon, M.-C. Daniel, A. Kaiba, P. Guionneau, S. Brandès and J.-P. Sutter, *J. Am. Chem. Soc.*, 2007, **129**, 13872–13878.
16 S. Chorazy, R. Podgajny, W. Nitek, T. Fic, E. Görlich, M. Rams and B. Sieklucka, *Chem. Commun.*, 2013, **49**, 6731–6733.
17 D. Pinkowicz, R. Podgajny, W. Nitek, M. Rams, A. M. Majcher, T. Nuida, S.-I. Ohkoshi and B. Sieklucka, *Chem. Mater.*, 2011, **23**, 21–31.
18 S.-I. Ohkoshi, S. Takano, K. Imoto, M. Yoshikiyo, A. Namai and H. Tokoro, *Nat. Photonics*, 2014, **8**, 65–71.
19 J. Zhang, S. Chen, H. Valle, M. Wong, C. Austria, M. Cruz and X. Bu, *J. Am. Chem. Soc.*, 2007, **129**, 14168–14169.
20 A. Gheorghe, B. Strudwick, D. M. Dawson, S. E. Ashbrook, S. Woutersen, D. Dubbeldam and S. Tanase, *Chem. – Eur. J.*, 2020, **26**, 13957–13965.
21 K. Qian, X.-C. Huang, C. Zhou, X.-Z. You, X.-Y. Wang and K. R. Dunbar, *J. Am. Chem. Soc.*, 2013, **135**, 13302–13305.
22 K. Nakabayashi, S. Chorazy, Y. Miyamoto, T. Fujimoto, K. Yazawa, D. Takahashi, B. Sieklucka and S.-I. Ohkoshi, *CrystEngComm*, 2016, **18**, 9236–9242.
23 C. F. Macrae, I. Sovago, S. J. Cottrell, P. T. A. Galek, P. McCabe, E. Pidcock, M. Platings, G. P. Shields, J. S. Stevens, M. Towler and P. A. Wood, *J. Appl. Crystallogr.*, 2020, **53**, 226–235.
24 M. F. A. Hendrickx, V. S. Mironov, L. F. Chibotaru and A. Ceulemans, *Inorg. Chem.*, 2004, **43**, 3142–3150.
25 A. Dees, A. Zahl, R. Puchta, N. J. R. van Eikema Hommes, F. W. Heinemann and I. Ivanović-Burmazović, *Inorg. Chem.*, 2007, **46**, 2459–2470.
26 V. W.-W. Yam, K. H.-Y. Chan, K. M.-C. Wong and N. Zhu, *Chem. – Eur. J.*, 2005, **11**, 4535–4543.
27 P. Li, J. M. Maier, J. Hwang, M. D. Smith, J. A. Krause, B. T. Mullis, S. M. S. Strickland and K. D. Shimizu, *Chem. Commun.*, 2015, **51**, 14809–14812.
28 N. Bridonneau, J. Long, J. L. Cantin, J. von Bardeleben, S. Pillet, E. E. Bendeif, D. Aravena, E. Ruiz and V. Marvaud, *Chem. Commun.*, 2015, **51**, 8229–8232.
29 M. Magott, O. Stefańczyk, B. Sieklucka and D. Pinkowicz, *Angew. Chem., Int. Ed.*, 2017, **56**, 13283–13287.
30 X. Qi, S. Pillet, C. de Graaf, M. Magott, E.-E. Bendeif, P. Guionneau, M. Rouzières, V. Marvaud, O. Stefańczyk, D. Pinkowicz and C. Mathonière, *Angew. Chem., Int. Ed.*, 2020, **59**, 3117–3121.
31 X. Qi, P. Guionneau, E. Lafon, S. Perot, B. Kauffmann and C. Mathonière, *Magnetochemistry*, 2021, **7**, 97.
32 M. Magott, M. Reczyński, B. Gaweł, B. Sieklucka and D. Pinkowicz, *J. Am. Chem. Soc.*, 2018, **140**, 15876–15882.
33 M. Magott, B. Gaweł, M. Sarewicz, M. Reczyński, K. Ogorzały, W. Makowski and D. Pinkowicz, *Chem. Sci.*, 2021, **12**, 9176–9188.
34 N. Ozaki, H. Tokoro, Y. Hamada, A. Namai, T. Matsuda, S. Kaneko and S.-I. Ohkoshi, *Adv. Funct. Mater.*, 2012, **22**, 2089–2093.
35 F. J. Birk, D. Pinkowicz and K. R. Dunbar, *Angew. Chem., Int. Ed.*, 2016, **55**, 11368–11371.
36 F. Luo, C. Yan, L. Dang, R. Krishna, W. Zhou, H. Wu, X. Dong, Y. Han, T.-L. Hu, M. O'Keeffe, L. Wang, M. Luo, R.-B. Lin and B. Chen, *J. Am. Chem. Soc.*, 2016, **138**, 5678–5684.
37 B. Van de Voorde, B. Bueken, J. Denayer and D. De Vos, *Chem. Soc. Rev.*, 2014, **43**, 5766–5788.
38 M. Atzori, G. L. J. A. Rikken and C. Train, *Chem. – Eur. J.*, 2020, **26**, 9784–9791.
39 M. Atzori, I. Breslavetz, K. Paillot, K. Inoue, G. L. J. A. Rikken and C. Train, *J. Am. Chem. Soc.*, 2019, **141**, 20022–20025.